

Seismic damage analysis due to near-fault multipulse ground motion

Guan Chen^{1,2}  | Jiashu Yang³ | Ruohan Wang^{1,2} | Kaiqi Li⁴ | Yong Liu²  | Michael Beer^{1,5,6}

¹Institute for Risk and Reliability, Leibniz Universität Hannover, Hannover, Germany

²State Key Laboratory of Water Resources Engineering and Management, Wuhan University, Wuhan, P.R. China

³School of Civil Engineering, Xi'an University of Architecture and Technology, Xi'an, P.R. China

⁴Department of Civil and Environmental Engineering, The Hong Kong Polytechnic University, Hong Kong, P.R. China

⁵Institute for Risk and Uncertainty and School of Engineering, University of Liverpool, Liverpool, UK

⁶International Joint Research Center for Resilient Infrastructure & International Joint Research Center for Engineering Reliability and Stochastic Mechanics, Tongji University, Shanghai, P.R. China

Correspondence

Guan Chen, Institute for Risk and Reliability, Leibniz Universität Hannover, Hannover 30167, Germany.
Email: guan.chen@irz.uni-hannover.de

Kaiqi Li, Department of Civil and Environmental Engineering, The Hong Kong Polytechnic University, Hung Hom, Kowloon, Hong Kong, China. Email: kqcee.li@polyu.edu.hk

Funding information

National Natural Science Foundation of China, Grant/Award Number: U22A20596; International Joint Research Platform Seed Fund Program of Wuhan University, Grant/Award Number: WHUZZJJ202207; China Scholarship Council; Sino-German (CSC-DAAD) Postdoc Scholarship Program

Abstract

Near-fault pulse-like ground motion is a significant class of seismic records since it tends to cause more severe damage to structures than ordinary ground motions. However, previous researches mainly focus on single-pulse ground motions. The multipulse ground motions that exist in records receive rare attention. In this study, an analysis procedure is proposed to investigate the effect of multipulse ground motions on structures by integrating finite element analysis and an identification method that features each pulse in the multipulse ground motion satisfying the same evaluation criteria. First, the Arias intensity, wavelet-based cumulative energy distribution, and response spectra of identified non-, single-, and multipulse ground motions are compared. Then, the seismic damage on frame structures, a soil slope, and a concrete dam under non-, single-, and multipulse ground motions are analyzed. Results show that the spectral velocity of multipulse ground motions is significantly greater than those of non- and single-pulse ground motions and potentially contains multiple peaks in the long-period range. Seismic damage evaluation indicates that the maximum interstory drift of frame structures with high fundamental periods under multipulse ground motions is about twice that of nonpulse ground motions. Similar characteristics also exist in the soil slope and the concrete dam. Therefore, multipulse ground motions potentially cause more severe damage to structures compared to non- and single-pulse ground motions. The findings of this study facilitate the recognition of the increased seismic demand imposed by the multipulse ground motion in engineering practices, provide new possibilities for ground motion selection in seismic design validation, and shed new light on seismic hazard and risk analysis in near-fault regions.

KEYWORDS

multipulse ground motion, near-fault earthquake, pulse-like ground motion, response spectrum, seismic damage analysis, seismic risk

This is an open access article under the terms of the [Creative Commons Attribution-NonCommercial-NoDerivs](https://creativecommons.org/licenses/by-nc-nd/4.0/) License, which permits use and distribution in any medium, provided the original work is properly cited, the use is non-commercial and no modifications or adaptations are made.

© 2023 The Authors. *Earthquake Engineering & Structural Dynamics* published by John Wiley & Sons Ltd.

1 | INTRODUCTION

Near-fault pulse-like ground motion is one of the hot spot issues in earthquake engineering since it potentially causes more severe damage to structures than ordinary ground motion (termed nonpulse ground motion in this study).^{1–3} This phenomenon was first discovered at the Port Hueneme earthquake in 1957,⁴ and further verified by following near-source earthquakes, such as 1995 Kobe Earthquake,⁵ 1999 Chi-Chi Earthquake,⁶ 2018 Hualien Earthquake,⁷ and 2023 Turkey-Syria Earthquake.⁸ These near-fault earthquakes effectively expand the pulse-like ground motion database and advance relevant research, such as the seismological mechanism of pulse generation,⁹ pulse-like ground motion identification,^{10,11} and simulation,^{12,13} and seismic damage analysis.^{1,14} However, current studies mainly focus on single-pulse ground motion. As a particular class of seismic records in near-fault regions, the multipulse ground motion is rarely considered. Therefore, the objective of this study is to facilitate recognizing the potential of near-fault multipulse ground motions on structural damage compared to non- and single-pulse ground motions.

Identifying the pulse-like ground motion is the prerequisite for relevant studies. To effectively extract the pulse-like ground motion from recorded databases, lots of identification methods are proposed, such as wavelet-based methods¹⁰ and energy-based methods.^{15,16} However, most of them focus on single-pulse ground motion identification. Only few investigations for multipulse ground motion are conducted. For example, Lu et al.¹⁷ proposed an iteration scheme to identify the multipulse ground motion based on wavelet transform. Chen et al.^{18,19} used Hilbert–Huang transform to extract multiple pulses in ground motion and analyzed the characteristics of multipulse ground motions. Although some methods have been developed, the identification criteria of multipulse ground motions are still in debate. Most previous studies, limited by signal processing techniques, consider the trend terms or long-period but low-amplitude parts of ground motions as multiple pulses. We believe that the attenuation part of the ground motion should be excluded. Hence, a generalized continuous wavelet transform method is proposed in the authors' previous study,¹¹ which can effectively identify the multipulse ground motion and avoid the influences of other factors. Similar to the criteria in most studies, this method classifies the nonpulse and pulse-like ground motions by whether a long-period and high-amplitude part exists in ground motion velocity. The identification of single- and multipulse ground motion is based on the number of pulses in velocity. If the ground motion velocity contains more than one pulses in velocity, it is considered a multipulse ground motion, otherwise a single-pulse ground motion. The proposed method features that each pulse in a multipulse ground motion should meet the same identification criteria. Pulse-like ground motions are identified from Chi-Chi, Taiwan earthquake at Pacific Earthquake Engineering Research (PEER) NGA-West2 database and applied in the seismic damage analysis.

The effects of pulse-like ground motion on structures is the key issue concerned in earthquake engineering. To investigate this issue, a number of seismic damage analyses of pulse-like ground motion have been carried out in various objects, such as slope,²⁰ gravity dam,²¹ tunnelling,⁶ building,^{22,23} and bridge.^{24,25} The analysis techniques are also diverse, like site investigations, laboratory experiments, and numerical simulations. Therein, numerical methods based on nonlinear dynamic response are widely applied due to their advantages in reflecting the nonstationary characteristics of pulse-like ground motion and their effectiveness and efficiency. The parameters of pulse-like ground motions, like the peak ground acceleration (PGA),²⁶ peak ground velocity (PGV),²⁷ the ratio of the pulse period and structural fundamental period,^{28–30} response spectrum characteristics,^{31,32} frequency-domain feature,^{33,34} and duration^{35,36} are also widely analyzed and quantitatively evaluated. That the pulse-like ground motion has potential side effects on structural safety is generally recognized.

However, most of these studies focus on single-pulse ground motions. The seismic damage analysis under multipulse ground motions is rare, while multipulse ground motions exist in records. Moreover, the multipulse signals may cause more severe damage than the single-pulse ones based on the tests using simple artificial signals, like triangle waves, square waves, and harmonic waves.^{2,28,37} Though multipulse ground motions are significant, the effects of recorded multipulse ground motions on structures are still unclear. To address this challenge, an identification method and an analysis procedure are formulated, where the identification method is utilized to detect the non-, single-, and multipulse ground motions from seismic databases, and the analysis procedure combines the finite element method and quantitative evaluation parameters to assess the seismic damage. To broaden the considerations of multipulse ground motions in engineering practice, three cases, including five frame structures with different fundamental periods, a soil slope, and a concrete dam, are exemplified to analyze the seismic damage under non-, single-, and multipulse ground motions. The seismic damage is quantitatively evaluated by various parameters accordingly.

The main contributions of this study are that the multipulse records are demonstrated to potentially cause more severe damage to structures compared to non- and single-pulse ground motions. Moreover, this phenomenon is observed for

various structural systems (including slopes, dams, and frame structures) and material properties (including soil, concrete, and steel). This finding helps to reveal the adverse impacts of multipulse ground motion in engineering practices, to broaden the wider considerations of multipulse ground motions in seismic hazard and risk analysis at near-fault regions, and to select ground motion in seismic design.

The organization of this work is as follows: the identification, selection, and intensity measures characteristics of non-, single-, and multipulse ground motions from the Chi-Chi, Taiwan earthquake are analyzed in Section 2. Three cases, involving frame structures, a soil slope, and a concrete dam, are illustrated in Sections 3–5, respectively. The seismic damage due to non-, single-, and multipulse ground motions is elaborated accordingly. The necessity of pulse-like ground motion classification, its implication for seismic design, and the caveats of this study are discussed in Section 6. The main conclusions are drawn in Section 7.

2 | GROUND MOTIONS DATABASE

2.1 | Pulse-like ground motion identification

The identification method proposed in the authors' previous work¹¹ is adopted to detect the non-, single-, and multipulse ground motions. This method identifies pulse-like ground motions by integrating the convolution analysis and evaluation parameters (energy ratio and Pearson correlation coefficient). A brief introduction of the identification procedure is as follows: it first applies the maximum absolute value of convolution results between the pulse model and ground motion to locate potential pulses, then judges whether the pulse meets the requirement of energy ratio, and finally excludes false identification with the correlation coefficient. Key points of the method are explained below.

The convolution analysis is applied since the maximum absolute value can effectively reflect the peak value and shape characteristics of a pulse. From the perspective of signal processing, the convolution (see Equation 1) can be regarded as a linear time-invariant (LTI) system, where $g(t)$ is the unit impulse response, $f(t)$ is the input signal, and $(f * g)(t)$ is the output signal.

$$(f * g)(t) = \langle f(t), g(t) \rangle = \int f(\tau) \cdot g(t - \tau) d\tau \quad (1)$$

where $(f * g)(t)$ is the integral of products between the “unit” of the input signal and the unit impulse response algebraically.

As the unit impulse response is confirmed (i.e., pulse model in the method), the value of $(f * g)(t)$ can reflect two characteristics of the “unit” of the input signal, that is, the amplitude and the shape. Moreover, the absolute value of $(f * g)(t)$ increases with the amplitude value and the similarity in shape between the pulse model and the “unit” of the input signal. Hence, the maximum absolute value of $(f * g)(t)$ is obtained on conditions that the “unit” of the input signal contains the local peak amplitude and is similar to the pulse model in the period. In other words, the maximum absolute convolution result is obtained when the identified pulse contains the local PGV and is similar to the pulse model in the period. This is the theoretical core of the proposed method to identify multipulse ground motions.

The wavelet basis “db4” is adopted as the pulse model referring to the study of Baker,¹⁰ which is one of the most popular identification methods in single-pulse ground motion. High energy in a pulse is one of the most common features of pulse-like ground motion, which is widely applied as an evaluation criterion in identification.¹⁵ Hence, this parameter is also utilized in this study to classify the nonpulse and pulse-like ground motions. Specifically, when a long-period and high-amplitude part accounts 30% energy of the whole signal, it is regarded as a pulse, and the ground motion is deemed as a pulse-like ground motion accordingly. Finally, the correlation coefficient is introduced to exclude the false identification caused by the trend term and the long-period but low-amplitude part of ground motions. Besides, only the records whose PGV is greater than 30 cm/s are considered as pulse-like ground motions in the seismic damage analysis referring to the study of Baker.¹⁰ The number of long-period and high-amplitude parts in velocity that satisfies the same criteria above is utilized to distinguish sing- and multipulse ground motions. More details about the method are elaborated in the authors' previous study.¹¹

As one of the most famous near-source earthquakes, the Chi-Chi, Taiwan Earthquake recorded many near-fault pulse-like ground motions, thus selected as the database in this study. Based on the proposed method, seven multipulse ground motions were identified. Correspondingly, seven non- and single-pulse ground motions are randomly selected to conduct

TABLE 1 Information of selected ground motions from Chi-Chi, Taiwan Earthquake†.

No.	RSN	Direction	PGV_p (cm/s)	T_p (s)	E_r	S_{max}	T_s (s)	Type
1	1244	Vertical	—	—	—	1.01g	0.14	Nonpulse
2	1245	Horizontal 1	—	—	—	0.88g	0.09	Nonpulse
3	1377	Horizontal 1	—	—	—	1.01g	0.11	Nonpulse
4	1377	Horizontal 2	—	—	—	1.25g	0.11	Nonpulse
5	1377	Vertical	—	—	—	0.81g	0.61	Nonpulse
6	1380	Vertical	—	—	—	1.08g	0.11	Nonpulse
7	1498	Vertical	—	—	—	0.84g	1.01	Nonpulse
8	1244	Horizontal 1	65.0	3.3	0.46	0.85g	0.17	Single-pulse
9	1244	Horizontal 2	109.0	5.0	0.72	0.89g	0.91	Single-pulse
10	1479	Horizontal 1	43.6	6.2	0.58	1.23g	0.45	Single-pulse
11	1481	Horizontal 1	56.7	6.9	0.66	0.95g	0.75	Single-pulse
12	1481	Vertical	32.3	5.3	0.80	0.92g	0.25	Single-pulse
13	1489	Horizontal 1	53.5	10.1	0.80	0.80g	0.17	Single-pulse
14	1506	Horizontal 1	37.2	6.7	0.48	1.16g	0.60	Single-pulse
15	1489	Horizontal 2	41.1/62.3	8.6/6.0	0.43/0.45	0.93g	0.26	Multipulse
16	1493	Horizontal 2	38.9/46.3	8.5/6.8	0.50/0.39	1.01g	0.69	Multipulse
17	1495	Horizontal 2	34.8/38.9	8.8/4.5	0.41/0.34	0.93g	0.63	Multipulse
18	1498	Horizontal 2	49.5/53.5	11.3/6.8	0.42/0.48	1.11g	0.38	Multipulse
19	1499	Horizontal 2	41.0/44.0	7.9/7.2	0.44/0.46	1.03g	0.27	Multipulse
20	1506	Horizontal 2	56.2/60.2	6.3/4.7	0.34/0.38	1.63g	0.60	Multipulse
21	1527	Horizontal 2	35.7/42.9	6.5/7.3	0.36/0.41	0.78g	0.39	Multipulse

†RSN—"Record Sequence Number" in PEER NGA-West2 flatfile; Horizontal 1/Horizontal 2/Vertical—the direction defined in PEER NGA-West2 flatfile; PGV_p —peak ground velocity of the pulse part (i.e., the identified pulse part of the original ground motion, as shown in Figures 1 and 2; T_p —pulse period; E_r —the energy ratio between the pulse part and the original ground motion; S_{max} —the maximum value of spectral acceleration, where the damping ratio is set to 5%, and the response spectra are calculated after the PGA is scaled to 0.3g; T_s —the period in the spectral acceleration corresponding to S_{max} ; Type—the types of non-, single-, and multipulse ground motion are based on the proposed identification method.

a comparative study. The information on these ground motions is listed in Table 1. The pulse-related parameters, including PGA of the pulse part (PGV_p), pulse period (T_p), and energy ratio (E_r), are provided based on the proposed method. Examples of the nonpulse (RSN 1498 vertical), single-pulse (RSN 1481 Horizontal 1), and multipulse (RSN 1498 Horizontal 2) ground motions are depicted in Figure 1. Other selected multipulse ground motions are plotted in Figure 2. It is worth noting that the PGA of all ground motions was scaled to 0.3g and then as input ground motion for seismic damage evaluation in case studies.

2.2 | Arias intensity and frequency-domain features

The Arias intensity and wavelet-based energy distribution are analyzed to characterize the time- and frequency-domain features of non-, single-, and multipulse ground motions, respectively. The normalized Arias intensity of selected ground motions in Table 1 is shown in Figure 3A. Owing to the limitations of Fourier transform in time-frequency conversion, which uses the infinite trigonometric signal to fit a signal in Hilbert space, the results are easily interfered by noises and would change with any mutation on the time domain.³⁸ Hence, the wavelet packet transform is utilized to conduct time-frequency conversion in this study due to the advantages of great resolution on both time and frequency domains.³⁹

For signal $S(x)$ in Hilbert space $L^2(\mathbb{R})$, the wavelet packet transform can be expressed as Equations (2) and (3).

$$S(t) = \sum_{j=0}^{2^i-1} f_{i,j}(t_j) \quad (2)$$

$$f_{i,j}(t_j) = \sum_{k=0}^m d_{i,j}^{(k)} \phi_{i,j}(t) \quad (3)$$

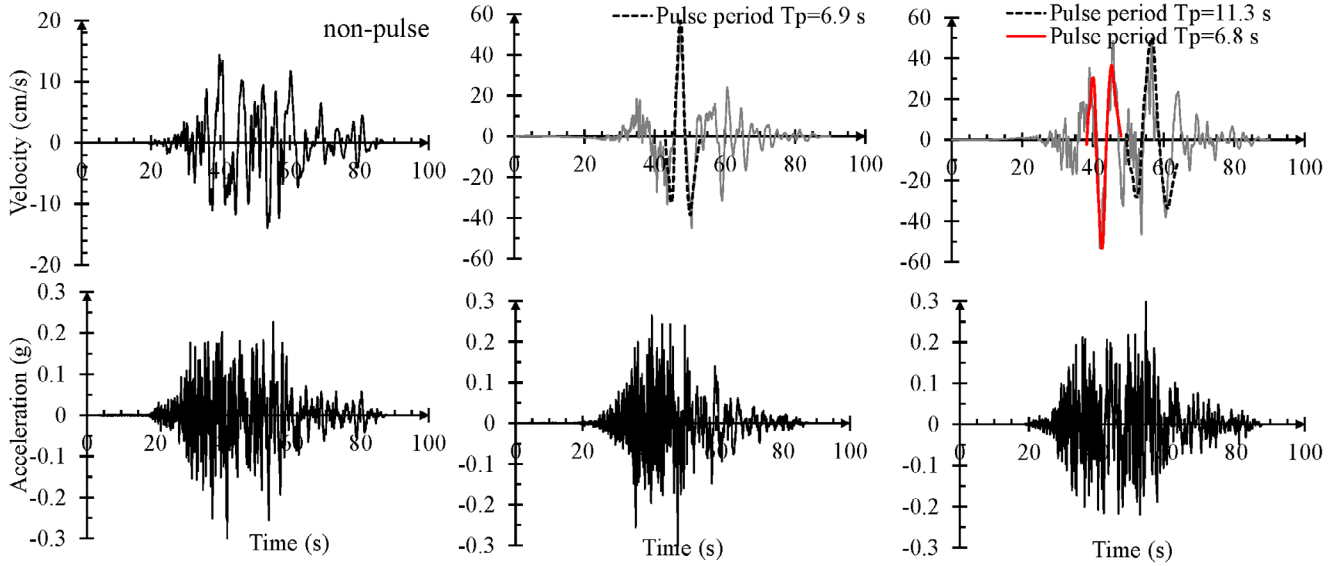


FIGURE 1 Examples for nonpulse (left), single-pulse (middle), and multipulse (right) ground motions in Chi-Chi, Taiwan Earthquake at PEER NGA-West2 database. Each pulse in multipulse ground motions satisfies the same identification criteria.

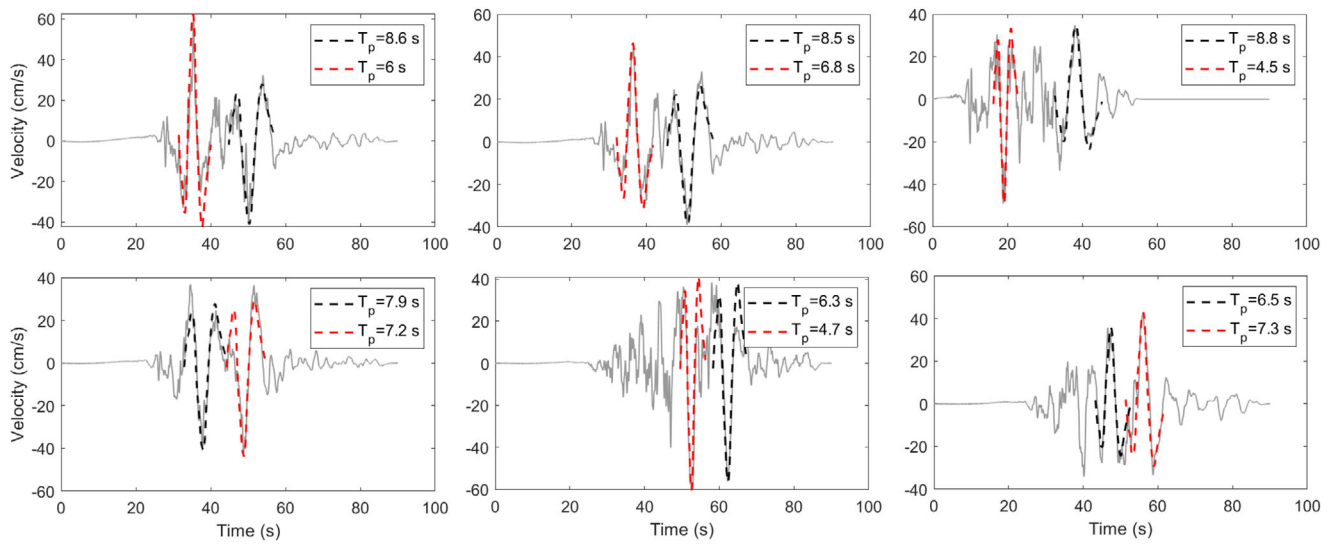


FIGURE 2 Other multipulse ground motions identified in Chi-Chi, Taiwan Earthquake.

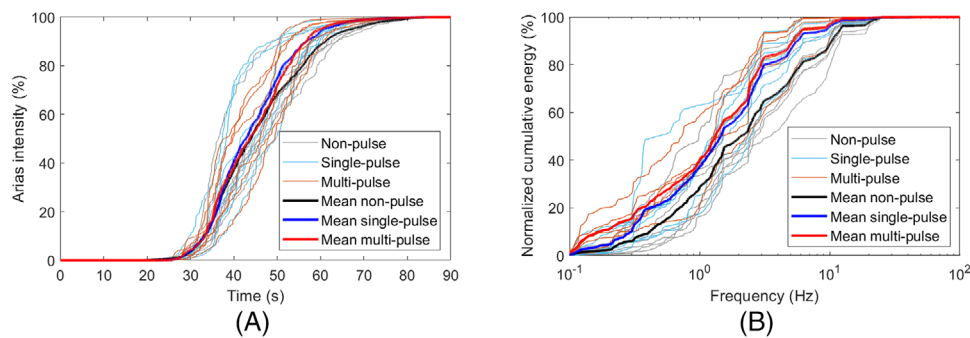


FIGURE 3 (A) Arias intensity and (B) wavelet-based normalized cumulative energy of selected ground motions in Table 1.

where $f_{i,j}(t_j)$ is the projection of $S(t)$ in wavelet space; $\phi_{i,k}(t)$ is the wavelet function that is the standard orthogonal basis of wavelet space; $d_{i,j}^{(k)}$ is the wavelet coefficient; i is the scale parameter; j is the wavelet packet subspace; k is the translation parameter. m is the discrete sampling point of the signal.

The wavelet-based frequency-domain energy is calculated by Equation (4).

$$P_{i,j} = \frac{\sum_{k=1}^m |d_{i,j}^{(k)}|^2}{\sum_{k=1}^{2^i-1} \sum_{k=1}^m |d_{i,j}^{(k)}|^2} \quad (4)$$

where $\sum_{k=1}^m |d_{i,j}^{(k)}|^2$ presents the energy at the frequency band corresponding to $f_{i,j}(t_j)$ in wavelet packet space.

The normalized cumulative energy C_s is calculated by Equation (5).

$$C_s = \frac{\sum_{j=1}^s P_{i,j}}{\sum_{j=1}^{2^i} P_{i,j}} \quad (5)$$

Based on Equations (2)–(5), the normalized cumulative energy in the frequency domain of selected ground motions is shown in Figure 3B. From Figure 3, the significant duration (D_{5-75}) is 22.3 s (31.0–53.3 s), 19.3 s (30.1–50.4 s), and 19.9 (30.9–50.8 s) for the average non-, single-, and multipulse ground motion, respectively. The significant frequency band (corresponding to energy from 5 to 75%) is 4.8 Hz (0.3–5.1 Hz), 2.7 Hz (0.2–2.9 Hz), and 2.5 Hz (0.1–2.6 Hz) for the average non-, single, and multi-pulse ground motion, respectively. Generally speaking, the Arias intensity of pulse-like and nonpulse ground motion present slight distinctions in local but follow the same trend on the whole. The significant frequency band of pulse-like ground motion is shorter than that of nonpulse ground motion. The pulse-like ground motion has more energy at frequency ranges of less than 1 Hz. Especially for the multipulse ground motion, the energy at the very low-frequency range (0.1–0.2 Hz) is significantly higher than non- and single-pulse ground motions.

2.3 | Response spectrum

The 5% damped spectral velocity and spectral acceleration of selected ground motions are calculated, shown in Figure 4A,B, respectively. The average response spectrum of non-, single-, and multipulse ground motion is also separately provided in the diagram. It shows that (i) the spectral velocity of multipulse ground motions is significantly greater than that of non- and single-pulse ground motions; moreover, it potentially contains multiple peaks at high-period ranges. This feature may cause adverse effects on structures with high fundamental periods. (ii) The maximum value for the average spectral acceleration of non-, single-, and multipulse ground motions is similar, that is 0.98, 0.97, and 1.06g, respectively. However, the period (T_s) corresponding to the maximum spectral acceleration varies between the nonpulse and pulse-like ground motions. The T_s of nonpulse ground motion is around 0.1 s, but that of the pulse-like ground motion is about 0.4–0.8 s.

3 | CASE 1: SEISMIC DAMAGE ON FRAME STRUCTURES

3.1 | Model description

To understand the effects of multipulse ground motions on structures with various fundamental periods, five typical 3D frame structures with different fundamental periods ($T_1 = 0.3, 0.6, 1, 36,$ and 5 s) are analyzed according to the Code For Seismic Design of Buildings (GB 50011-2010) in China. All these structures are modeled based on the OpenSees platform using displacement-based nonlinear beam–column elements.

Different materials and heights are adopted to obtain various fundamental periods. For structures of $T_1 = 0.3, 0.6,$ and 1 s, the reinforced concrete is used and described by a uniaxial Kent–Scott–Park model⁴⁰ with degraded linear unloading/reloading stiffness and no tensile strength.⁴¹ Besides, a uniaxial bilinear model with kinematic hardening is adopted to characterize the nonlinearity in both rebars and steel members. For structures of $T_1 = 3$ and 5 s, the steel frame structures are adopted. The damping ratio of the first two modes of concrete and steel structures are assumed to be 0.05 and 0.03, respectively. Live loads are considered in the form of nonstructural masses. An example of the typical stress–strain

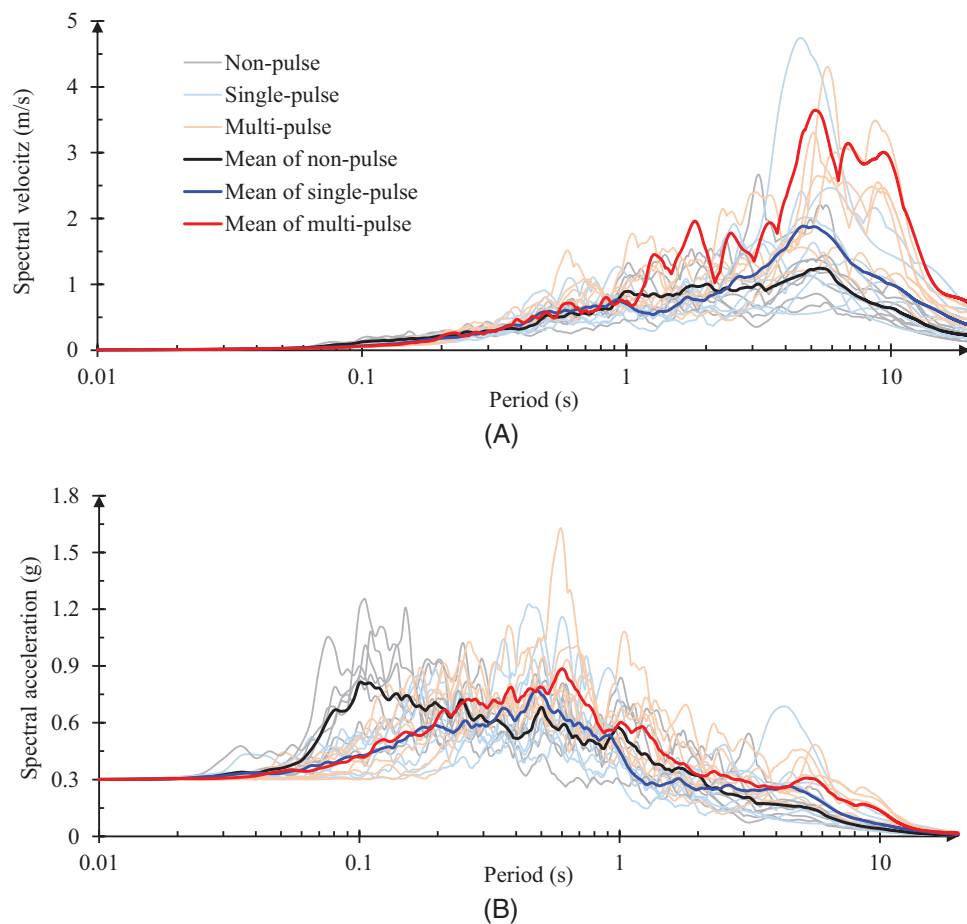


FIGURE 4 (A) Spectral velocity and (B) spectral acceleration of selected ground motions. The PGA of all ground motions is scaled to 0.3g before the response spectrum analysis. The damping ratio is 5%.

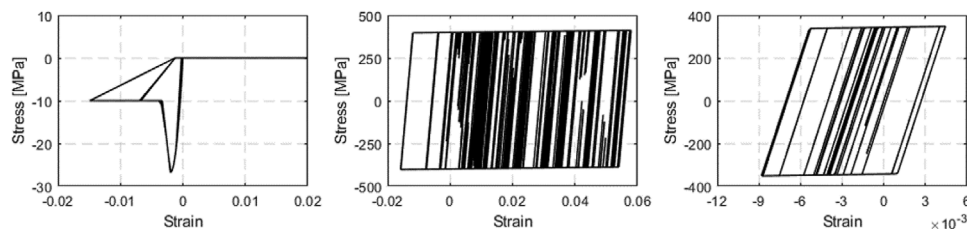


FIGURE 5 Stress-strain hysteresis loop for the concrete (left) and steel rebar (middle) in $T_1 = 0.3, 0.6, \text{ and } 1 \text{ s}$ structures and for the steel (right) in $T_1 = 3 \text{ and } 5 \text{ s}$ structures.

hysteresis loop of the concrete and steel is provided in Figure 5 to illustrate the material properties. Basic information on the structures is listed in Table 2. Diagrams and layouts of the structures with $T_1 = 0.3$ and 3 s are provided as examples and shown in Figure 6A,B, respectively.

The frame structures are subjected to unidirectional seismic excitation in this study. In particular, the seismic excitation is considered along the directions featured by translations of the first mode. Furthermore, to take into account the effect of slabs, rigid diaphragms are assumed in all the frame structures. More details of the structural models, such as the layout of standard floors, the section sizes of columns and beams, and the corresponding parameters, can be found in Chen et al.³³

3.2 | Seismic damage evaluation

The maximum interstory drift is adopted to quantify the seismic damage on frame structures. The maximum drift in each story and the entire structure are provided in Figures 7 and 8, respectively. Results show that (i) the maximum

TABLE 2 Structures information.

T_1	Story height \times number	Geometrical parameters
0.3 s	4.5 m \times 2	One and two bays are along the X and Y directions, respectively. The width of each bay is 4.5 m.
0.6 s	4.5 m \times 4	One and two bays are along the X and Y directions, respectively. The width of each bay is 4.5 m.
1 s	4.5 m \times 6	Two bays are in both the X and Y directions and the bay widths are 3.0 and 4.0 m, respectively.
3 s	3.7 m \times 12	Two and three bays are along the X and Y directions, respectively. The width of each bay is 6.1 m.
5 s	3.8 m \times 16	Three and five bays are in the X and Y directions, and the bay widths are 7.3 and 6.4 m, respectively.

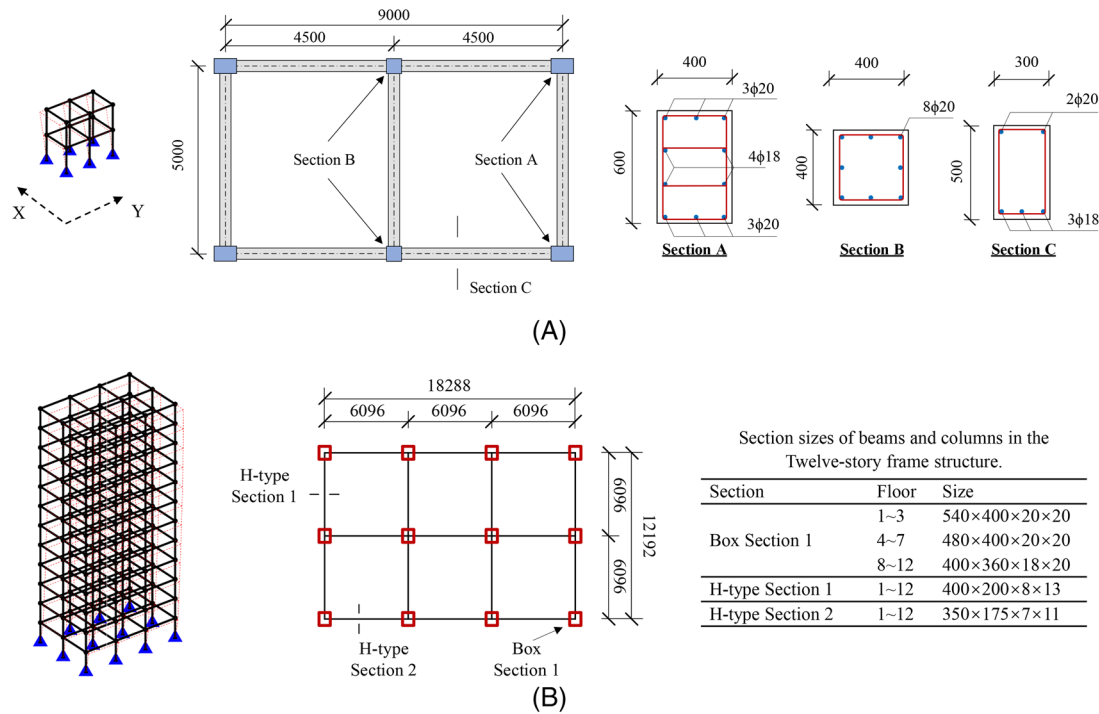


FIGURE 6 Diagrams and layouts of standard floors and section characteristics of the frame structures. (A) Two-story concrete frame structure; (B) 12-story steel frame structure.

drift occurs at different story levels for structure with different fundamental periods but at the same story level for the same structure subjected to different types of ground motions. For example, the maximum drift is at the bottom for the steel frame structures. (ii) However, the value of the maximum drift of the same structure varies under different types of ground motions. As shown in Figure 8, the maximum interstory drift under multipulse ground motions is generally larger than those of non- and single-pulse ground motions. Specifically, the average maximum drift of structure with $T_1 = 0.3$ s subjected to non-, single-, and multipulse ground motions is 26.0, 30.0, and 32.5 mm, respectively; that of $T_1 = 0.6$ s is 48.0, 45.6, and 55.1 mm; that of $T_1 = 1$ s is 65.1, 58.0, and 74.0 mm; that of $T_1 = 3$ s is 50.5, 35.5, and 66.4 mm; and that of $T_1 = 5$ s is 75.8, 83.2, and 128.7 mm. Therefore, multipulse ground motions tend to cause more severe damage to frame structures compared to non- and single-pulse ground motions, especially to structures with higher fundamental periods (greater than 1 s). (iii) The maximum drift of different structures in Figure 8 is caused by various ground motions. For the multipulse ground motions, the RSN1506H2 results in the maximum drift of the structure when $T_1 = 5$ s; however, the RSN1527H2 leads to the maximum drift to the structure when $T_1 = 3$ s. This indicates that the increased seismic demand caused by multipulse ground motion is rooted in the inherent multipulse characteristics of ground motion velocity, rather than being influenced by a specific individual record. The ground motion information that causes the maximum drift for each structure are listed in the Supporting Information.

In addition, to test the effects of material strength on seismic response, we varied the compression strength of concrete (for structures with $T_1 = 0.3$, 0.6, and 1.0 s) and the yield strength of steel (for structures with $T_1 = 3.0$ and 5.0 s) to 0.8 and 1.2 times of their original values. While the seismic response of structures varies across three cases, similar results to Figure 8 were obtained on the maximum drift of the entire structures. Hence, the increased seismic demand caused

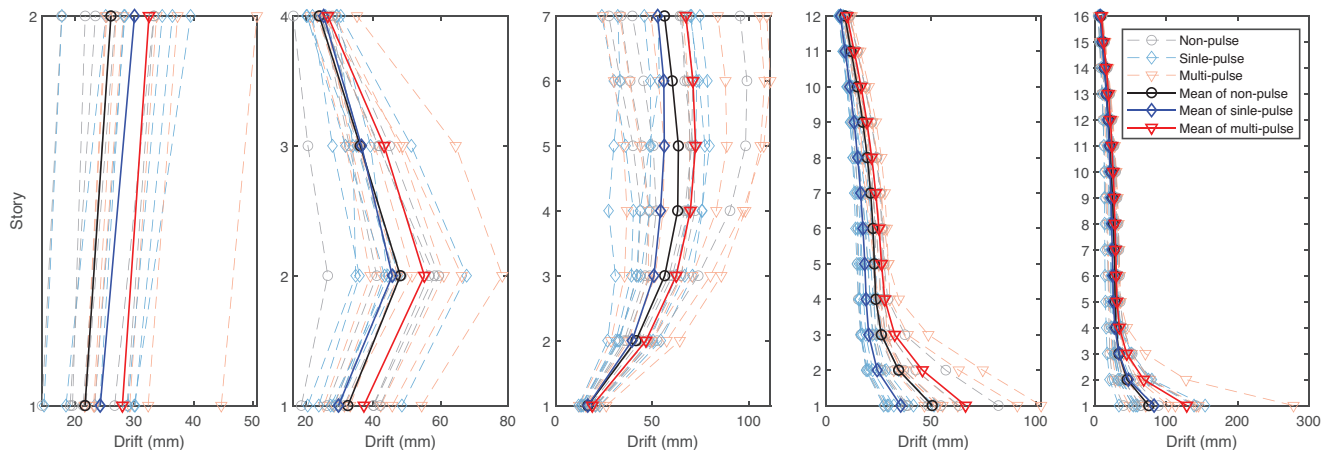
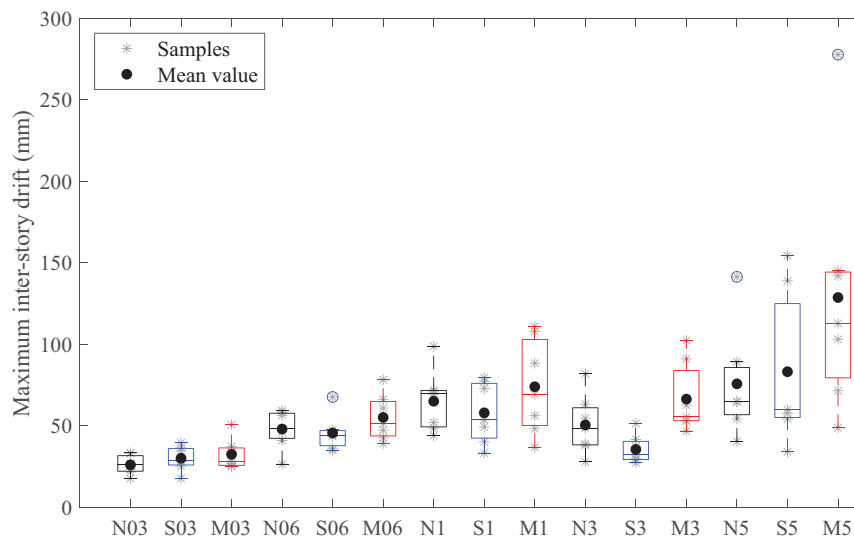


FIGURE 7 Maximum drift at each story level. Relationship between the story level and fundamental period is listed in Table 2.

FIGURE 8 Boxplot about the maximum interstory drift of five frame structures subjected to non-, single-, and multipulse ground motions. The “N,” “S,” and “M” in the x-axis denote non-, single-, and multipulse ground motion, respectively. The number “03,” “06,” “1,” “3,” and “5” means the structural fundamental period. For example, the sign “N03” indicates the structure with a fundamental period of 0.3 s under nonpulse ground motions.



by multipulse ground motion is evident for structures with different material attributes. The detailed calculations are provided in the Supporting Information.

Therefore, multipulse ground motions consistently lead to more severe damage to frame structures, regardless of the varying structural fundamental periods and material properties. It should be noted that the comparison of seismic damage under non-, single-, and multipulse ground motions is performed under consistent PGA conditions.

4 | CASE 2: SEISMIC DAMAGE ON SOIL SLOPE

4.1 | Model description

An unsaturated clayey soil slope subjected to non-, single-, and multipulse ground motions is analyzed, where the dynamic unified hardening constitutive model proposed by Luo et al.⁴² is utilized to characterize the unsaturated clayey soil properties. A three-dimensional finite element analysis is conducted by combining a coupling-based hydro-mechanical analysis based on ABAQUS software with user subroutines written in FORTRAN. The model consists of 9840 elements, which are all eight-node elements with reduced integration (C3D8R). Material properties of clay soil in Lou et al.⁴² are used, as listed in Table 3. The geometric dimensions and finite element mesh of the slope model are depicted in Figure 9. The mass-proportional coefficient and stiffness-proportional coefficient of Rayleigh damping for the slope model are assumed

TABLE 3 Mechanical parameters of soil materials.

Parameters	λ (-)	κ (-)	M (-)	ν (-)	N (-)	α (kPa)	p^c (kPa)	κ_s (-)	ρ (g/cm ³)
Value	0.136	0.018	1.0	0.3	1.217	90	100	0.0256	1.92

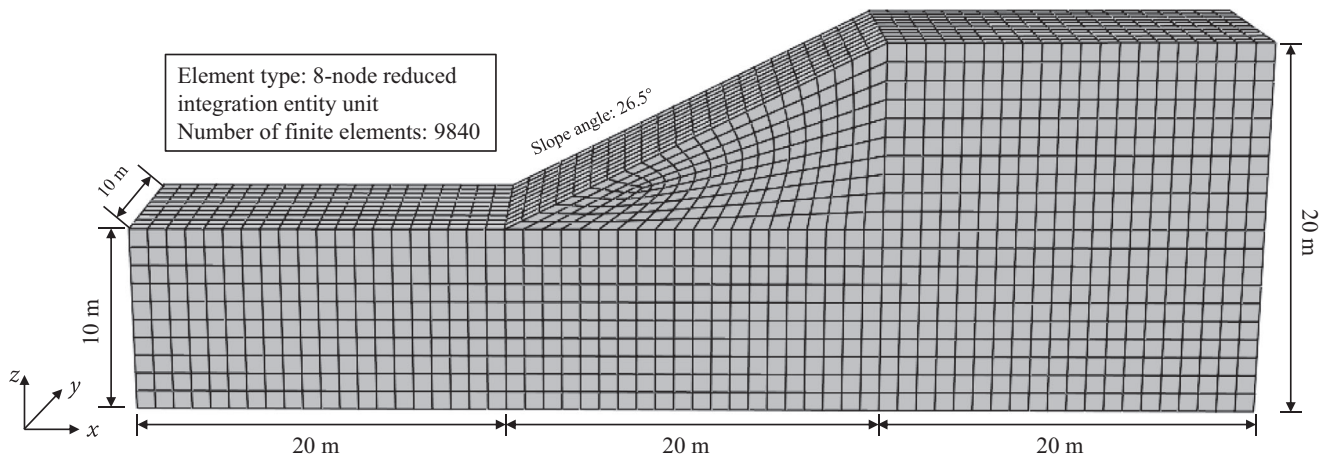


FIGURE 9 Finite element model of the clayey soil slope.

to be 2.4354 and 0.0008, respectively, which adopt the values given by Nguyen et al.⁴³ The boundary conditions of the model are as follows: the upper boundary is considered a free face, while the surrounding boundary is absorption; the bottom is rigid and the ground motion is applied along the x -axis direction. Besides, the fundamental period of the slope is 1.32 s. More details of the slope model, such as the corresponding physical parameters and the constitutive relationship, can be found in Wang et al.⁴⁴

4.2 | Seismic damage evaluation

The maximum displacement of the slope is analyzed, as shown in Figure 10. A boxplot (see Figure 11) is also provided to illustrate the maximum displacement of slope subjected to non-, single-, and multipulse ground motions. The results reveal that the variation tendencies for both maximum displacement U_t and maximum displacement U_x at X -axis direction are similar. Specifically, the mean value of U_t for the slope model subjected to non-, single-, and multipulse ground motions is 6.9, 7.2, and 11.3 cm, respectively; that of U_x is 4.4, 4.5, and 6.0 cm, respectively. It can be seen that the mean values of U_t and U_x calculated under single-pulse ground motions are slightly larger than those calculated under nonpulse ground motion loading. However, the mean values of U_t and U_x subjected to multipulse ground motion are significantly larger than those under non- and single-pulse ground motions. The value of U_x under multipulse ground motions is almost 1.6 times the values of the other two cases, indicating that this special class of ground motions is prone to result in more serious damage on slopes.

There is another interesting phenomenon in Figure 10 that the location of maximum displacement under non-, single-, and multipulse ground motions moves from the toe to the top of the slope. This may relate to the various site amplification of slope to different types of ground motion. However, more comprehensive studies are required to explore the mechanism and summarize solid results, which will be conducted in future works.

5 | CASE 3: SEISMIC DAMAGE ON CONCRETE DAM

5.1 | Model description

As one of the few real-world concrete gravity dams damaged during earthquakes, the Koyna dam has been extensively analyzed. The constitutive model and material parameters for the dam are also widely verified.^{45,46} Based on these studies, a finite element model for Koyna Dam is investigated to analyze the effects of multipulse ground motions on dam damage.

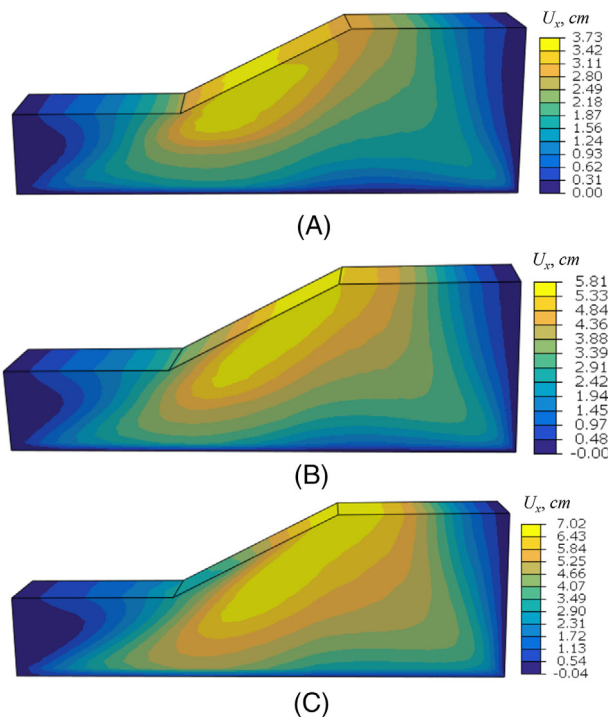


FIGURE 10 Example contours of maximum displacement in X-axis direction subjected to (A) non-, (B) single-, and (C) multipulse ground motions.

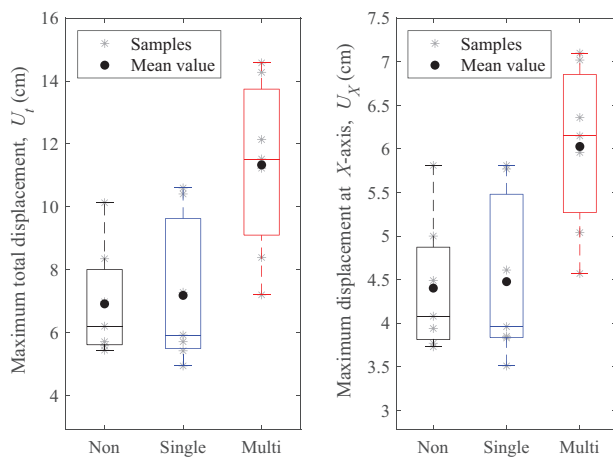


FIGURE 11 Boxplot about the total (left) and X-axis direction (right) maximum displacement of slope subjected to non-, single-, and multipulse ground motions.

The seismic damage analysis of the dam can be simplified as a plane stress problem according to the study of Lee et al.⁴⁶ The geometric parameters and the mesh of the model are shown in Figure 12. The model contains 760 elements, and the element type is CPS4R in ABAQUS software. The boundary conditions are set as follows: the bottom is the rigid boundary, where the ground motions are imposed; the interaction between the reservoir and dam is considered with Westergaard’s method, which means the water move with the dam, and the force in the dam is a denominated value with $7/8\rho_w\sqrt{h_w(h_w - y)}$, where h_w is the depth of water level; y is the position of the dam; ρ_w is the density of water. The calculation procedure is divided into two steps. The responses under gravity and static water pressure are computed at first. Then, nonlinear dynamic response analysis is conducted by inputting ground motions.

According to former studies,^{46,47} the concrete damaged plasticity model can effectively describe the force–displacement relationship of the Koyna Dam under seismic ground motion. The concrete damaged plasticity model is briefly explained

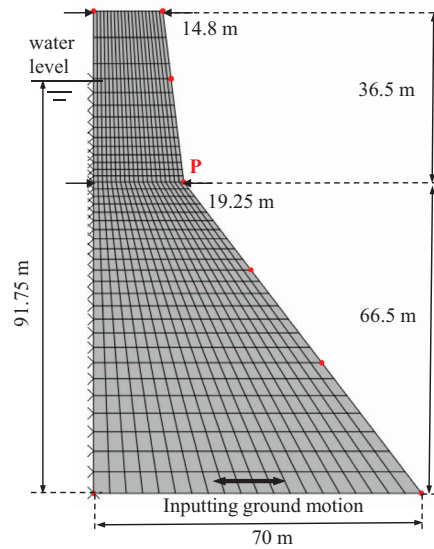


FIGURE 12 Numerical model of Koyna Dam.

as follows. Its uniaxial stress and strain relationship is expressed in Equation (6).

$$\begin{aligned}\sigma_t &= (1 - d_t)E_0(\epsilon_t - \tilde{\epsilon}_t^{pl}) \\ \sigma_c &= (1 - d_c)E_0(\epsilon_c - \tilde{\epsilon}_c^{pl})\end{aligned}\quad (6)$$

where σ_t and σ_c are the tensile and compressive stresses, respectively; d_t and d_c are the tensile and compressive damage variables, respectively; E_0 is the elastic modulus; ϵ_t and ϵ_c are the total tensile and compressive strain, respectively; $\tilde{\epsilon}_t^{pl}$ and $\tilde{\epsilon}_c^{pl}$ are the plastic tensile and compressive strains, respectively.

The yield functions in Lee and Fenves⁴⁶ are applied, and shown in Equation (7).

$$\begin{aligned}F &= \frac{1}{1 - \alpha}(\bar{q} - 3\alpha\bar{p} + \beta(\tilde{\epsilon}^{pl})\langle \hat{\sigma}_{max} \rangle - \gamma\langle \hat{\sigma}_{max} \rangle) - \bar{\sigma}_c(\tilde{\epsilon}^{pl}) = 0 \\ \alpha &= \frac{(\sigma_{b0}/\sigma_{c0}) - 1}{(2\sigma_{b0}/\sigma_{c0}) - 1}; 0 \leq \alpha \leq 0.5 \\ \beta &= \frac{\bar{\sigma}_c(\tilde{\epsilon}_c^{pl})}{\bar{\sigma}_t(\tilde{\epsilon}_t^{pl})}(1 - \alpha) - (1 + \alpha) \\ \gamma &= \frac{3(1 - K_c)}{2K_c - 1}\end{aligned}\quad (7)$$

where, $\hat{\sigma}_{max}$ is the maximum principal effective stress; σ_{b0}/σ_{c0} is the ratio of initial equibiaxial compressive yield stress to initial uniaxial compressive yield stress (the default value is 1.16); K_c is the ratio of the second stress invariant on the tensile meridian to that on the compressive meridian at initial yield for any given value of the pressure invariant p such that the maximum principal stress is negative, and it must satisfy the condition $0.5 \leq K_c \leq 1$ (the default value is 2/3); $\bar{\sigma}_t(\tilde{\epsilon}_t^{pl})$ and $\bar{\sigma}_c(\tilde{\epsilon}_c^{pl})$ are the effective tensile and compressive cohesion stresses, respectively.

The dam material parameters are listed in Table 4. To avoid the side effects of gridding on calculation accuracy, the fracture energy cracking criterion is adopted to describe the tensile characteristics of the dam after tension strength. The tensile properties after tension strength, which are described by displacement, are listed in Table 5. This study only considers the tensile damage, that is, d_c is always 0.

The damping is generally required in dynamic analysis for describing the energy dissipation. The Rayleigh damping is used in this study, which is controlled by the mass matrix and stiffness matrix, as shown in Equation (8).

$$[C] = \alpha[M] + \beta[K] \quad (8)$$

TABLE 4 Material parameters of Koyna Dam.

Parameter	Value
Density	2643 kg/m ³
Young's modulus	31027 MPa
Poisson's ratio	0.15
Dilation angle	36.31°
Tensile failure stress	2.9 MPa
Compressive initial yield stress	13.0 MPa
Compressive ultimate stress	24.1 MPa

TABLE 5 Concrete tensile properties.

Cracking displacement (×10 ⁻⁴ m)	Tensile stress (MPa)	Tensile damage variable
0	2.9	0
0.66185	1.94393	0.381217
1.2286	1.30305	0.617107
1.73427	0.873463	0.763072
2.2019	0.5855	0.853393
2.64718	0.392472	0.909282
3.08088	0.263082	0.943865
3.5105	0.176349	0.965265
3.94138	0.11821	0.978506
4.37744	0.0792388	0.9867
4.82165	0.0531154	0.99177

where C is the Rayleigh damping matrix; M is the mass matrix; K is the stiffness matrix; α and β are the coefficients for Rayleigh damping, which are related to the damping ratio and mode frequency (see Equation 9).

$$\xi_i = \frac{\alpha}{2\omega_i} + \frac{\beta\omega_i}{2} \quad (9)$$

where ξ_i is the damping ratio associated with the i th mode frequency; ω_i is the i th mode frequency.

Based on the study of Chopra et al.,⁴⁵ the first mode frequency of Koyna Dam (ω_1) is 19.27 rad/s. That is, the fundamental period of the dam is 0.33 s. Besides, the damping ratio (ξ) is taken as 3%. Only the relationship between damping ratio and mass is considered, that is $\alpha = 0$. Then, based on Equation (8), $\beta = 2\xi/\omega_1$, and the value of β is 3.23×10^{-3} .

5.2 | Seismic damage evaluation

The seismic dynamic responses of the dam are analyzed with selected ground motions. Two typical groups of results are shown in Figures 13 and 14. The maximum plastic strain (see Figure 13) indicates that the basic crack direction caused by non-, single-, and multipulse ground motion coincides well. The crack begins in the neck point P (see Figure 12) and proceeds along the lower-left direction. However, the fracture degree varies. The crack under the multipulse ground motion almost crossed the whole dam. The fracture under single-pulse ground motion is less than that under multipulse ground motions, and the fracture in nonpulse ground motion is the least.

The tensile damage variable in Figure 14 shows that the damage location caused by the non-, single-, and multipulse ground motion is consistent, and mainly at the bottom and neck of the dam. However, the damaged ratio varies. Generally speaking, the damaged area under single-pulse ground motion is less than that of multipulse ground motion and greater than that of nonpulse ground motion.

Two parameters are employed to quantitatively characterize the seismic damage under non-, single-, and multipulse ground motions. First, the displacement response is one of the critical parameters in antiseismic design.⁴⁸ Thus, the maximum plastic strain of the dam is selected as one of the damage evaluation parameters. This parameter can effectively

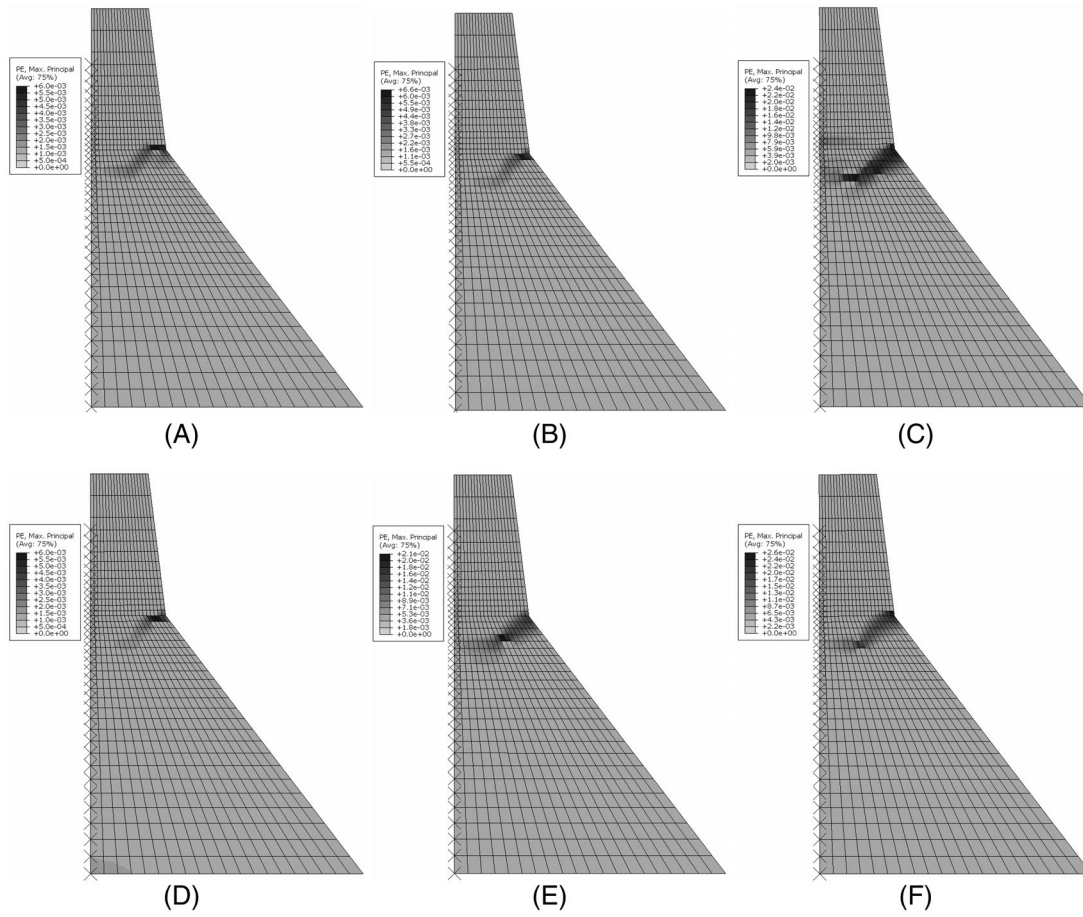


FIGURE 13 Maximum plastic strain of dam under non-, single-, and multipulse ground motion. (A) and (D) is under the nonpulse ground motion, that is RSN 1380 Vertical and RSN 1498 Vertical, respectively. (B) and (E) is under the single-pulse ground motion, that is RSN 1244 Horizontal 2 and RSN 1481 Horizontal 1, respectively. (C) and (F) is under the multipulse ground motion, that is RSN 1498 Horizontal 2 and RSN 1506 Horizontal 2, respectively.

assess the tensile cracking degree at the local susceptible area. Second, a global damage index (see Equation 10) is defined in this study to evaluate the global damage of the dam.

$$\lambda = \frac{n_d}{N} \quad (10)$$

where λ is the global damage index; n_d is the number of elements the tensile damage variable is greater than 0.8; N is the total amount element of the model, which is 760 in this study.

The boxplot about the global damage index and the peak value of maximum plastic strain of the dam under non-, single-, and multipulse ground motions is shown in Figure 15. It indicates that the global damage of the dam caused by multipulse ground motions is generally greater than those of non- and single-pulse ground motions. The average tensile damage area caused by multipulse ground motions is about 1.4 times that of single-pulse ground motions, and 2.2 times that of nonpulse ground motions. The peak value of the maximum plastic strain also shows similar characteristics. The peak strain caused by the single-pulse ground motion is less than that of multipulse ground motions, and greater than that of nonpulse ground motions. It implies that the crack caused by multipulse ground motion is larger than the other two cases. Combined with Figure 13, the multipulse ground motion often results in longer cracks. This indicates that damage caused by the multipulse ground motion is more likely to penetrate the whole dam.

Therefore, similar to the seismic damage on frame structures and the soil slope, multipulse ground motions also potentially cause more severe damage on concrete dams than non- and single-pulse ground motions.

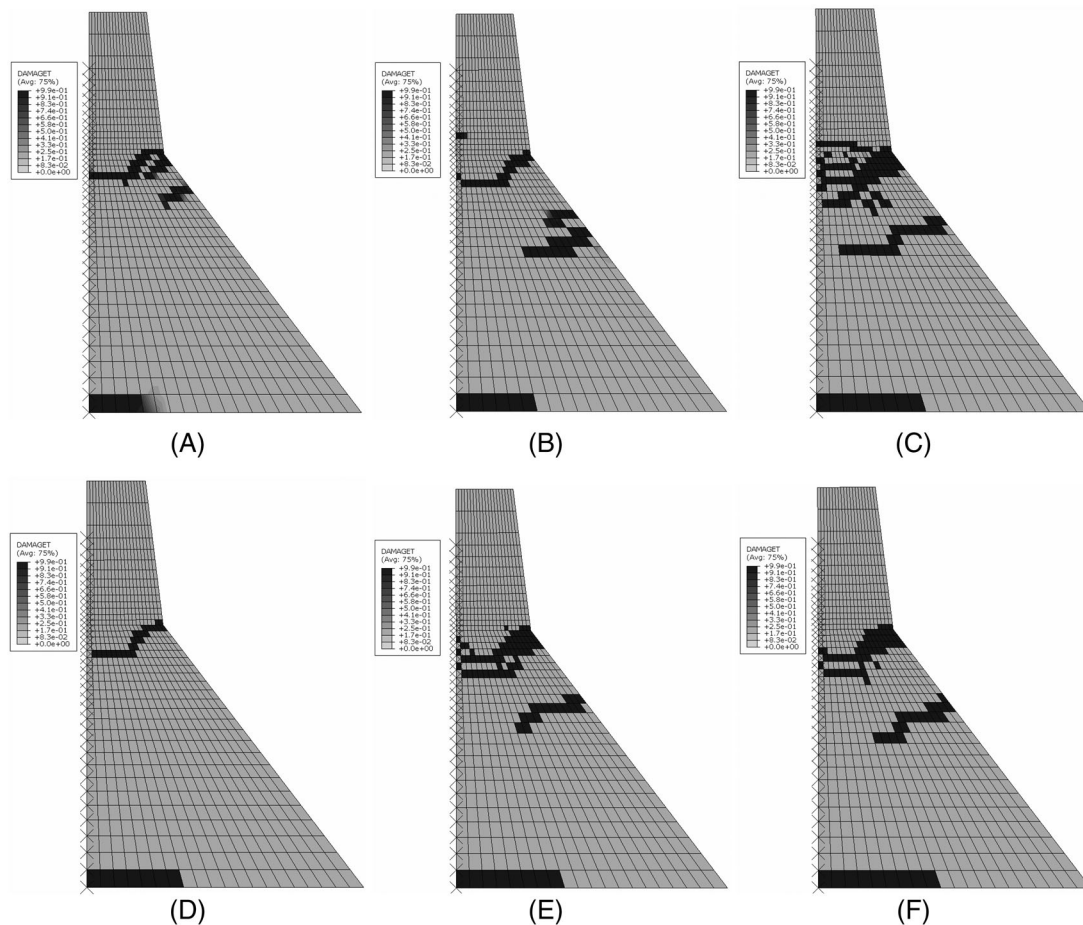


FIGURE 14 Tensile damage variable of dam under non-, single-, and multipulse ground motion. (A) and (D) is under the nonpulse ground motion, that is RSN 1380 Vertical and RSN 1498 Vertical, respectively. (B) and (E) is under the single-pulse ground motion, that is RSN 1244 Horizontal 2 and RSN 1481 Horizontal 1, respectively. (C) and (F) is under the multipulse ground motion, that is RSN 1498 Horizontal 2 and RSN 1506 Horizontal 2, respectively.

6 | DISCUSSIONS

This study organized three different engineering issues to illustrate that multipulse ground motions require increased seismic demand compared to non- and single-pulse excitation. To further facilitate wider considerations of multipulse ground motion in engineering practices, the necessity of multipulse ground motion classification, the implications of multipulse ground motion in seismic design, and some caveats of this study are discussed.

Similar to the motivation of classification of pulse-like ground motion, the multipulse ground motion is classified as a particular set due to its existence in seismic databases and the potential to cause more severe damage to structures. To demonstrate these two points, two complementary works are carried out. The previous work develops a novel method to identify the multipulse ground motion in seismic databases,¹¹ and this study highlights the potential of multipulse records in causing structural damage. To the authors' best knowledge, this study is the first one to clearly define the effects of multipulse ground motion on seismic damage, and to illustrate that multipulse ground motions tend to cause more severe damage on structures compared to non- and single-pulse ground motions. This information can be applied to inform the risk assessment and retrofit of structures in seismic-prone regions, ultimately improving the safety of buildings and infrastructure. Therefore, the classification of multipulse ground motion is necessary in terms of engineering applications.

As for the implications in seismic design, multipulse ground motion provides new possibilities for ground motion selection in near-fault regions. For instance, when validating seismic designs, particularly for megastructures, it is often necessary to consider ground motions that may cause the worst damage.⁴⁹ In such cases, multipulse ground motion should be taken into account. Furthermore, when sufficient records are observed in earthquakes, the multipulse ground motion can help target spectrum design in near-fault regions.

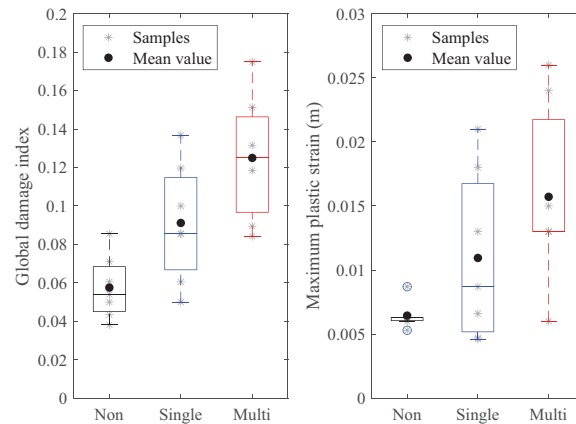


FIGURE 15 Boxplot about the global damage index (left) and the maximum plastic strain (right) of the dam subjected to non-, single-, and multipulse ground motions.

There are also some caveats in this study. (i) This study demonstrates increased seismic demands imposed by the multipulse records using different structural systems (including a slope, a dam, and frame structures) and materials (including soil, concrete, and steel). Moreover, different evaluation parameters are adopted for different structural systems in seismic damage evaluation. This strategy helps engineers and scholars in different fields recognize the adverse effects of multipulse ground motion on structural safety. However, the mechanism of how multipulse ground motion leads to greater maximum drift in frame structures, increased displacement in slopes, and more cracks in dams is less explored in this study. These are crucial issues and will be conducted in future works. In short, this study recognized that multipulse ground motions require large seismic demands on structures, but more work is needed to comprehensively understand all important aspects of this issue. (ii) This study does not comprehensively consider the randomness of ground motions limited by the amounts of multipulse records. However, the effects of the stochastic property of ground motion should be considered to summarize more universal conclusions.³ Relevant work will also be conducted in the future when more multipulse records are available. (iii) This study does not involve the seismological mechanism of multipulse ground motion generation. However, this is another essential component to further broaden the application of multipulse records.

7 | CONCLUSIONS

As a particular class of seismic records in the near-fault earthquake, the multipulse ground motion is rarely considered in seismic damage analysis compared to single-pulse ground motions. To demonstrate the effects of multipulse ground motion on seismic damage, an identification method valid for both single- and multipulse ground motions and an analysis procedure that integrates finite element method and evaluation parameters are formulated. The Arias intensity, frequency contents, and response spectra among non-, single-, and multipulse ground motions are compared. The seismic damage under these ground motions is also elaborated with frame structures, a soil slope, and a concrete dam as examples. Two aspects of conclusions are derived.

On the one hand, based on the identification method that features each pulse in multipulse ground motions satisfying the same identification criteria, seven groups of non-, single-, and multipulse ground motions are selected. The intensity measures comparison shows the Arias intensity of non-, single- and multipulse ground motions is basically similar; the wavelet-based frequency-domain energy distribution, however, is diverse. Specifically, the 5%–75% energy corresponding frequency band of nonpulse ground motion is about twice of pulse-like ground motion, and the pulse-like ground motion has more energy at a frequency of less than 1 Hz. Furthermore, the spectral velocity of multipulse ground motion is generally greater than that of non- and single-pulse ground motion, and may contain multi-peaks in the long-period range, which may cause side effects on structures with high fundamental periods.

On the other hand, the seismic damage evaluation shows that multipulse ground motions are prone to cause more severe damage to various structural systems than non- and single-pulse ground motions. Specifically, the maximum interstory drift under multipulse ground motion is significantly greater than that of non- and single-pulse ground motion for the frame structures, regardless of the varying structural fundamental periods and material properties. Similar phenomena also exist in seismic damage to soil slopes and concrete dams. Therefore, as a particular class of seismic records in

near-fault earthquakes that may cause the worst damage, the multipulse ground motions should be underlined in relevant seismic damage analyses. Moreover, the increased seismic demand imposed by multipulse ground motion compared to non- and single-pulse ground motions provides new possibilities for ground motion selection in seismic design.

ACKNOWLEDGMENTS

This research is supported by the National Natural Science Foundation of China (Grant No. U22A20596) and the International Joint Research Platform Seed Fund Program of Wuhan University (Grant No. WHUZZJJ202207). Ruohan Wang has received the financial support from China Scholarship Council (CSC). Guan Chen would like to thank the financial support of Sino-German (CSC-DAAD) Postdoc Scholarship Program.

CONFLICT OF INTEREST STATEMENT

The authors declare no conflicts of interest.

DATA AVAILABILITY STATEMENT

The raw earthquake ground motions used in the study can be freely downloaded at PEER NGA-West2 database (<https://ngawest2.berkeley.edu/>). Specifically, the ground motion is accessible by searching the earthquake names in the “Event Name” text box, where the earthquake named “Chi-Chi, Taiwan” is used.

ORCID

Guan Chen  <https://orcid.org/0000-0002-3709-1247>

Yong Liu  <https://orcid.org/0000-0003-1006-7842>

REFERENCES

- Sehhati R, Rodriguez-Marek A, ElGawady M, Cofer WF. Effects of near-fault ground motions and equivalent pulses on multi-story structures. *Eng Struct*. 2011;33(3):767-779.
- Li S, Zhang F, Wang Jq, Alam MS, Zhang J. Effects of near-fault motions and artificial pulse-type ground motions on super-span cable-stayed bridge systems. *J Bridge Eng*. 2017;22(3):04016128.
- Chen G, Liu Y, Beer M. Effects of response spectrum of pulse-like ground motion on stochastic seismic response of tunnel. *Eng Struct*. 2023;289:116274.
- Housner G, Hudson DE. The Port Hueneme earthquake of March 18, 1957. *Bull Seismol Soc Am*. 1958;48(2):163-168.
- Kawase H. The cause of the damage belt in Kobe: “the basin-edge effect,” constructive interference of the direct S-wave with the basin-induced diffracted/Rayleigh waves. *Seismol Res Lett*. 1996;67(5):25-34.
- Wang W, Wang T, Su J, Lin C, Seng C, Huang T. Assessment of damage in mountain tunnels due to the Taiwan Chi-Chi earthquake. *Tunn Undergr Space Technol*. 2001;16(3):133-150.
- Kuo CH, Huang JY, Lin CM, Hsu TY, Chao SH, Wen KL. Strong ground motion and pulse-like velocity observations in the near-fault region of the 2018 Mw 6.4 Hualien, Taiwan, earthquake. *Seismol Res Lett*. 2019;90(1):40-50.
- Chen G. Report on pulse-like ground motions in the Feb 2023 Turkey earthquakes. Preprint. 2023. <http://doi.org/10.13140/RG.2.2.31375.25767>
- Somerville PG, Smith NF, Graves RW, Abrahamson NA. Modification of empirical strong ground motion attenuation relations to include the amplitude and duration effects of rupture directivity. *Seismol Res Lett*. 1997;68(1):199-222.
- Baker JW. Quantitative classification of near-fault ground motions using wavelet analysis. *Bull Seismol Soc Am*. 2007;97(5):1486-1501.
- Chen G, Liu Y, Beer M. Identification of near-fault multi-pulse ground motion. *Appl Math Modell*. 2023;117:609-624.
- Mavroeidis GP, Papageorgiou AS. A mathematical representation of near-fault ground motions. *Bull Seismol Soc Am*. 2003;93(3):1099-1131.
- Chen G, Beer M, Liu Y. Modeling response spectrum compatible pulse-like ground motion. *Mech Syst Sig Process*. 2022;177:109177.
- Chandramohan R, Baker JW, Deierlein GG. Quantifying the influence of ground motion duration on structural collapse capacity using spectrally equivalent records. *Earthq Spectra*. 2016;32(2):927-950.
- Zhai C, Chang Z, Li S, Chen Z, Xie L. Quantitative identification of near-fault pulse-like ground motions based on energy. *Bull Seismol Soc Am* 2013;103(5):2591-2603.
- Mukhopadhyay S, Gupta VK. Directivity pulses in near-fault ground motions—I: identification, extraction and modeling. *Soil Dyn Earthq Eng*. 2013;50:1-15.
- Lu Y, Panagiotou M. Characterization and representation of near-fault ground motions using cumulative pulse extraction with wavelet analysis. *Bull Seismol Soc Am*. 2014;104(1):410-426.
- Chen X, Wang D, Zhang R. Identification of pulse periods in near-fault ground motions using the HHT method. *Bull Seismol Soc Am*. 2019;109(6):2384-2398.
- Chen X, Wang D. Multi-pulse characteristics of near-fault ground motions. *Soil Dyn Earthq Eng*. 2020;137:106275.
- Pang R, Xu B, Kong X, Zhou Y, Zou D. Seismic performance evaluation of high CFRD slopes subjected to near-fault ground motions based on generalized probability density evolution method. *Eng Geol*. 2018;246:391-401.
- Yazdani Y, Alembagheri M. Nonlinear seismic response of a gravity dam under near-fault ground motions and equivalent pulses. *Soil Dyn Earthq Eng*. 2017;92:621-632.

22. Alonso-Rodríguez A, Miranda E. Assessment of building behavior under near-fault pulse-like ground motions through simplified models. *Soil Dyn Earthq Eng*. 2015;79:47-58.
23. Kalkan E, Kunnath SK. Effects of fling step and forward directivity on seismic response of buildings. *Earthq Spectra*. 2006;22(2):367-390.
24. Phan V, Saiidi MS, Anderson J, Ghasemi H. Near-fault ground motion effects on reinforced concrete bridge columns. *J Struct Eng*. 2007;133(7):982-989.
25. Yang S, Mavroeidis GP, Ucak A. Analysis of bridge structures crossing strike-slip fault rupture zones: a simple method for generating across-fault seismic ground motions. *Earthq Eng Struct Dyn*. 2020;49(13):1281-1307.
26. Dicleli M, Buddaram S. Effect of isolator and ground motion characteristics on the performance of seismic-isolated bridges. *Earthq Eng Struct Dyn*. 2006;35(2):233-250.
27. Yang D, Pan J, Li G. Non-structure-specific intensity measure parameters and characteristic period of near-fault ground motions. *Earthq Eng Struct Dyn*. 2009;38(11):1257-1280.
28. Alavi B, Krawinkler H. Behavior of moment-resisting frame structures subjected to near-fault ground motions. *Earthq Eng Struct Dyn*. 2004;33(6):687-706.
29. Alavi B, Krawinkler H. Strengthening of moment-resisting frame structures against near-fault ground motion effects. *Earthq Eng Struct Dyn*. 2004;33(6):707-722.
30. Mavroeidis G, Dong G, Papageorgiou A. Near-fault ground motions, and the response of elastic and inelastic single-degree-of-freedom (SDOF) systems. *Earthq Eng Struct Dyn*. 2004;33(9):1023-1049.
31. Malhotra PK. Response of buildings to near-field pulse-like ground motions. *Earthq Eng Struct Dyn*. 1999;28(11):1309-1326.
32. Somerville P. New developments in seismic hazard estimation. In: *Proceedings of the 6th International Conference on Seismic Zonation (6ICSZ)*. Palm Springs; 2000.
33. Chen G, Yang J, Liu Y, Kitahara T, Beer M. An energy-frequency parameter for earthquake ground motion intensity measure. *Earthq Eng Struct Dyn*. 2023;52(2):271-284.
34. Rathje EM, Abrahamson NA, Bray JD. Simplified frequency content estimates of earthquake ground motions. *J Geotech Geoenviron Eng*. 1998;124(2):150-159.
35. Zhang H, Zhang L, Wang H, Guan C. Influences of the duration and frequency content of ground motions on the seismic performance of high-rise intake towers. *Eng Fail Anal*. 2018;91:481-495.
36. Repapis CC, Mimoglou PP, Dimakopoulou VV, Psycharis IN, Taflampas IM. Efficient strong motion duration of pulse-like records for nonlinear structural analyses. *Earthq Eng Struct Dyn*. 2020;49(5):479-497.
37. Chang SP, Makris N, Whittaker AS, Thompson AC. Experimental and analytical studies on the performance of hybrid isolation systems. *Earthq Eng Struct Dyn*. 2002;31(2):421-443.
38. Chen G, Li QY, Li DQ, Wu ZY, Liu Y. Main frequency band of blast vibration signal based on wavelet packet transform. *Appl Math Modell*. 2019;74:569-585.
39. Chen G, Li K, Liu Y. Applicability of continuous, stationary, and discrete wavelet transforms in engineering signal processing. *J Perform Constr Facil*. 2021;35(5):04021060.
40. Scott B, Park R, Priestley M. Stress-strain behavior of concrete confined by overlapping hoops at low and high strain rates. *J Am Concr Inst*. 1982;79(1):13-27.
41. Karsan I, Jirsa J. Behavior of concrete under compressive loadings. *J Struct Div*. 1969;95(12):2543-2564.
42. Luo T, Chen D, Yao YP, Zhou AN. An advanced UH model for unsaturated soils. *Acta Geotech*. 2020;15(1):145-164.
43. Van Nguyen D, Kim D, Nguyen DD. Nonlinear seismic soil-structure interaction analysis of nuclear reactor building considering the effect of earthquake frequency content. *Structures*. 2020;26:901-914.
44. Wang R, Chen G, Liu Y, Beer M. Seismic reliability assessment framework for unsaturated soil slope under near-fault pulse-like ground motion. Under Review. 2023.
45. Chopra AK, Chakrabarti P. The Koyna earthquake and the damage to Koyna dam. *Bull Seismol Soc Am*. 1973;63(2):381-397.
46. Lee J, Fenves GL. A plastic-damage concrete model for earthquake analysis of dams. *Earthq Eng Struct Dyn*. 1998;27(9):937-956.
47. Zhang S, Wang G. Effects of near-fault and far-fault ground motions on nonlinear dynamic response and seismic damage of concrete gravity dams. *Soil Dyn Earthq Eng*. 2013;53:217-229.
48. Calvi G, Kingsley G. Displacement-based seismic design of multi-degree-of-freedom bridge structures. *Earthq Eng Struct Dyn*. 1995;24(9):1247-1266.
49. Takewaki I. A comprehensive review of seismic critical excitation methods for robust design. *Adv Struct Eng*. 2005;8(4):349-363.

SUPPORTING INFORMATION

Additional supporting information can be found online in the Supporting Information section at the end of this article.

How to cite this article: Chen G, Yang J, Wang R, Li K, Liu Y, Beer M. Seismic damage analysis due to near-fault multipulse ground motion. *Earthquake Engng Struct Dyn*. 2023;52:5099–5116. <https://doi.org/10.1002/eqe.4003>